

Manufacturing and characterization of an interpenetrating metal matrix composite reinforced with a 3D-printed metallic glass lattice structure (Ni60Nb20Ta20)

Kerstin Dittmann, Anna Trauth, Kay André Weidenmann

Angaben zur Veröffentlichung / Publication details:

Dittmann, Kerstin, Anna Trauth, and Kay André Weidenmann. 2023. "Manufacturing and characterization of an interpenetrating metal matrix composite reinforced with a 3D-printed metallic glass lattice structure (Ni60Nb20Ta20)." *Composite Structures* 327 (November): 117697. <https://doi.org/10.1016/j.compstruct.2023.117697>.

Manufacturing and characterization of an interpenetrating metal matrix composite reinforced with a 3D-printed metallic glass lattice structure

(Ni₆₀Nb₂₀Ta₂₀)

Kerstin Dittmann^[1], Anna Trauth^[1], Kay André Weidenmann^[1]

[1] Institute of Materials Resource Management (MRM), Augsburg University, Am Technologiezentrum 8, 86159 Augsburg, Germany

Corresponding author:

Kerstin Dittmann

Chair of Hybrid Composite Materials

Institute of Materials Resource Management (MRM)

Augsburg University

Am Technologiezentrum 8

86159 Augsburg, Germany

e-mail: kerstin.dittmann@mrm.uni-augsburg.de

phone: +49 (0) 821 598 - 69177

Abstract

Metallic glasses (MG) exhibit remarkable properties, like high strength, hardness, and elastic strain limit due their amorphous structure. But they also exhibit low ductility and brittle behavior, making them less suitable for monolithic components. Therefore, MG offer high potential for use as a reinforcing phase in a ductile matrix. Especially interpenetrating metal matrix composites (IMMCs) are suitable, since good interfacial adhesion can be achieved due to the metallic character of the MG and mechanical properties can be further enhanced by the interpenetrating structure. Temperature during manufacturing process must be below crystallization temperature of the MG. Until now, interpenetrating IMMCs have been manufactured by infiltrating the metal matrix foam with MG, requiring a high melting temperature of the matrix and thus excludes lightweight metals. In this work it was possible to infiltrate an open porous lattice structure of MG ($\text{Ni}_{60}\text{Nb}_{20}\text{Ta}_{20}$) due to its high crystallization temperature with AlSi12 by gas pressure infiltration resulting in a novel IMMC. X-ray diffraction measurements confirm that no crystallization occurred during infiltration. Micrographs show a good infiltration quality and interfacial bonding between both phases. An increase in Young's modulus of 28% and compressive strength in the IMMC can be achieved compared to the AlSi12-matrix.

Keywords:

Interpenetrating Metal Matrix Composite (IMMC); metallic glass (MG); mechanical properties; $\text{Ni}_{60}\text{Nb}_{20}\text{Ta}_{20}$; gas pressure infiltration

1 Introduction

Metal matrix composites (MMCs) are macroscopic composite materials consisting of a metallic matrix and a reinforcing phase. Typical reinforcing phases in MMCs are ceramic materials, which are mostly embedded in a light metal matrix [1]. The reinforcing phase can be in particle, fiber or as a 3-dimensional structure. 3-dimensional structures are also referred to as interpenetrating composites, in which each phase of the composite is topologically interconnected throughout the entire material volume [2]. MMCs offer the possibility to outperform monolithic components in mechanical properties such as specific stiffnesses as well as creep and fatigue behavior [1,3,4].

Metallic glasses have an amorphous structure and thus exhibit remarkable properties, such as high strength, hardness and elastic strain limit associated with the possibility of high elastic energy storage [5–7]. However, they also exhibit low ductility and consequently are prone to brittle fracture, which makes them less suitable for the use as monolithic structural components [8]. Therefore, they are more likely to be used as a reinforcing phase in a hybrid material, such as MMCs, with a ductile matrix to compensate for brittleness [9–11]. In several studies it has been proven that reinforcing with metallic glass increases the strength and Young's modulus of the metallic matrix [9,12,13] and maintains the plastic deformation capability under compressive loading [14]. Additionally, due to the metallic character of metallic glasses, it is potentially easier to realize an interfacial adhesion to a metallic matrix than by using a ceramic reinforcement phase [15,16]. However, the temperature in the manufacturing process of the composite must be lower than the crystallization temperature of the metallic glass to avoid undesirable crystallization and the associated loss of the mentioned properties. Since the manufacturing temperatures for metallic glass based MMCs must be low, MMCs reinforced with metallic glass are often produced by powder metallurgy. For this purpose, powdered metallic glass combined with the matrix is sintered by hot pressing. Several studies have shown that this manufacturing process is a good method to manufacture MMCs reinforced with particles of metallic glass [10,12,17]. Besides powder metallurgical manufacturing, there are already studies investigating the production of metallic glass based MMCs by gas pressure infiltration. In [13], metallic glass platelets of Ni-Nb-Ta alloy were infiltrated with an aluminum casting alloy under argon atmosphere without occurring crystallization. Also interpenetrating MMCs reinforced with metallic glass have been produced and investigated in several studies. In [18], a titanium foam was infiltrated with melted metallic glass and the composite was subsequently quenched. The X-ray diffraction (XRD) measurements showed single crystalline phases at the interfaces between titanium and the metallic glass. Nevertheless, compared to the monolithic glass or porous titanium, the MMC shows a significant increase in compressive strength and enhancement of plastic deformation capacity. In [19], porous tungsten was infiltrated with metallic glass. The subsequent XRD measurements did not show any

crystalline phases and the compressive strength and strain of the MMC exceeded those of the tungsten foam, as well as the monolithic metallic glass. However, so far only metal matrix foams have been infiltrated with metallic glass and not vice versa a metallic glass foam with metal matrix. This requires the second phase to have a much higher melting temperature than the metallic glass. Therefore, light metal materials such as aluminum and magnesium are not suitable for this process, since most metallic glasses have a higher melting temperature. In this case, the foam would have to be made of metallic glass, which requires that the metallic glass has a high crystallization temperature. In previous work [20], it was possible to manufacture this required open lattice structure of metallic glass with alloy composition $\text{Ni}_{60}\text{Nb}_{20}\text{Ta}_{20}$ by laser powder bed fusion (LPBF). The metallic glass exhibits a crystallization temperature of 694°C and is therefore high enough for an infiltration process with a light metal material.

In this work, the $\text{Ni}_{60}\text{Nb}_{20}\text{Ta}_{20}$ lattice structure was infiltrated with a eutectic AlSi12 matrix by a gas pressure infiltration process for the first time, resulting in a novel interpenetrating MMC reinforced with metallic glass. The AlSi12 matrix has a melting temperature of 577°C [21], which is far enough below the crystallization temperature of the metallic glass. Before and after the infiltration process XRD measurements were performed on the metallic glass to analyze the amorphous structure regarding crystallization. The microstructure and interfaces of the MMC were investigated and evaluated from micrographs using digital microscopy and energy dispersive X-ray (EDX) measurements with scanning electron microscopy (SEM). In addition, the elastic constants (Young's modulus, Poisson's ratio) were determined by ultrasound phase spectroscopy (UPS) and the mechanical properties were investigated by compression tests.

2 Experimental

2.1 Materials

In the study at hand, a metallic glass with alloy composition $\text{Ni}_{60}\text{Nb}_{20}\text{Ta}_{20}$ (TaNi39.1Nb20.7wt.-%), produced by Fraunhofer Institute IFAM (Dresden, Germany), was used as reinforcement phase. It obtained its amorphous structure through a powder gas atomization process by the company Nanoval GmbH & Co.KG (Berlin, Germany). The amorphous powder with particle size $d_{50}=44\mu\text{m}$ was further processed into an open-porous lattice structure with a volume fraction of 37% by LPBF. This process was conducted in cooperation with the research group "Production and Component Behavior" (Institute for Applied Materials – Materials Science and Engineering) at Karlsruhe Institute of

Technology. For a detailed description of the process of the lattice structure, the authors refer to [20]. An AlSi12 eutectic aluminum alloy was used as matrix material.

2.2 Gas pressure infiltration process

The interpenetrating composite was manufactured by gas pressure infiltration. For a detailed description of the equipment used, the authors refer to [22,23]. In the study at hand, the $\text{Ni}_{60}\text{Nb}_{20}\text{Ta}_{20}$ lattice structure with a size of $30 \times 30 \times 15 \text{ mm}^3$ was placed on the bottom of a cylindrical ceramic crucible so that it was in contact with the crucible only at its corners. A ceramic plate with a hole in the center was placed above the preform with some distance, and the AlSi12 ingots were placed on top. This should ensure uniform infiltration of the preform and reduce gas inclusions. Before starting the infiltration process, the infiltration chamber with the ceramic crucible inside was evacuated and purged with argon to avoid oxidation of the metallic glass. After evacuating again to a vacuum of 0.08 mbar, the infiltration chamber was heated up to a processing temperature of $T_p = 660^\circ\text{C}$ with a heating rate of 5.5 K/min. During heating, the vacuum in the infiltration chamber was held around 0.1 mbar. The processing temperature mentioned was chosen to be above the melting temperature of the eutectic AlSi12 matrix (577°C [21]) and below the crystallization temperature of the metallic glass (694°C [20]). The temperature was held for two hours to melt the AlSi12 ingots and homogenize the melt. Subsequently, an infiltration argon gas pressure of 40 bar was applied and held for 10 minutes before cooling down the infiltration chamber to room temperature. The solidified interpenetrating MMC was removed from the ceramic crucible for further characterization.

2.3 X-ray diffraction

XRD measurements were carried out on the metallic glass before and after infiltration to investigate the amorphous structure and to check if undesired crystallization would have taken place during infiltration. The measurements were conducted with a Seifert 3003 TT diffractometer provided by the Chair of Solid State Chemistry (Institute of Physics) at Augsburg University. A sample of the $\text{Ni}_{60}\text{Nb}_{20}\text{Ta}_{20}$ lattice structure before infiltration was manually milled into powder using a mortar. The infiltrated MMC was first placed in hydrochloric acid to etch out the AlSi12 matrix. Subsequently, the remaining $\text{Ni}_{60}\text{Nb}_{20}\text{Ta}_{20}$ lattice structure was also manually mortared. The XRD pattern was collected at room temperature in Bragg-Brentano geometry using $\text{Cu-K}\alpha$ radiation. The X-ray tube operated at 40 kV and 40 mA, scan range $10-60^\circ$, step width 0.02° , 40 scans per data point and 160 s integration time per degree.

2.4 Microscopy

A Keyence VHX-6000 digital microscope was used for the characterization of the microstructure by means of metallography. For this purpose, the samples were embedded in epoxy resin and afterwards grinded and polished, according to the preparation steps listed in Table 1. The samples were also used for SEM-EDX microanalysis of the interfaces. This was performed using a Prisma E SEM from ThermoFisher Scientific. The EDX points of a line spectrum analyses were measured with a voltage of 25 kV and electric current of 1 nA over a period of 30 seconds and an average of 16000 counts per second were detected.

Table 1: Grinding and polishing steps to prepare the samples for SEM-EDX microanalysis.

Grinding paper / polishing cloth	Suspension	Contact pressure (N)	Circulation (rpm)	Time (min)
SiC (P1200)	Water	25	Co-rotation 150/150	5:00
MD-Largo	Diamond, 9 μm	25	Co-rotation 150/150	3:30
MD-DAC	Diamond, 3 μm	20	Co-rotation 150/150	3:30
MD-DUR	Diamond, 1 μm	10	Co-rotation 100/110	3:30
MD-CHEM	OP-S	10	Counter-rotation 150/150	1:10

2.5 Ultrasound phase spectroscopy

UPS measurements were performed to determine the Young's modulus and the Poisson's ratio. The measurement and evaluation method used is described in detail in [24,25]. The investigated specimens of the infiltrated MMC have a cubic geometry ($5 \times 5 \times 5 \text{ mm}^3$) and to determine the density of the specimens, they were weighed with an Explorer EX225D (linearity $\pm 0.1 \text{ mg}$) from Ohaus and the volume was measured with a micrometer screw. The UPS measurements were performed using an electronic network analyzer of the type R3754A Advantest, connected with two pairs of longitudinal (Olympus, V122-RM, nominal central frequency 7.5 MHz) and transversal (Olympus, V155-RM, nominal central frequency 5.0 MHz) ultrasonic wave transducers. Amplitude and phase spectra were obtained in the frequency range from 10 kHz to 10 MHz. Each direction of one sample was measured three times with longitudinal waves, where the direction of wave propagation is parallel to polarization direction. Subsequently, each direction of one sample was measured with transversal waves, where the polarization direction is orthogonal to the direction of wave propagation, resulting in two directions of polarization. Each polarization direction was measured three times. This corresponds to nine

measurements per direction and a total of 27 measurements per sample [Table 2]. For this work, five samples were measured completely, and the results averaged.

Table 2: UPS measurements performed on each sample.

	Sensor	Wave propagation	Polarization	Measurements	Skizze
x-direction, E_1	V122	[100]	[100]	3	
	V155	[100]	[010]	3	
	V155	[100]	[001]	3	
y-direction, E_2	V122	[010]	[010]	3	
	V155	[010]	[001]	3	
	V155	[010]	[100]	3	
z-direction, E_3	V122	[001]	[001]	3	
	V155	[001]	[010]	3	
	V155	[001]	[100]	3	

2.6 Compression tests

Mechanical compression tests were carried out to investigate the mechanical strength of the infiltrated MMC at room temperature on a Zwick Kappa DS testing machine from Zwick/Roell with a maximum load cell capacity of 50kN. For this investigation, the cubic specimens of the UPS measurements were used after the UPS characterization. According to DIN 50106 [26], crosshead velocity was constantly set to 0.12mm/min, which corresponds to a nominal strain rate of $\dot{\epsilon} = 4 \cdot 10^{-4} s^{-1}$ and a pre-load of 20N was applied. The deformation was measured by digital image correlation (DIC) at a frame rate of 1Hz using a 12M ARAMIS (2D) system from GOM GmbH and evaluated with the associated software with a virtual extensometer.

3 Results and discussion

In the following chapter, the results of the infiltration process and characterization of the infiltrated MMC are presented and furthermore discussed.

3.1 Composite Manufacturing

Figure 1(a) shows the results of the XRD measurements carried out on the $Ni_{60}Nb_{20}Ta_{20}$ preform before and after infiltration to investigate the influence of the process on the amorphous structure of the metallic glass. Additionally, the XRD pattern of the unprocessed $Ni_{60}Nb_{20}Ta_{20}$ powder is included.

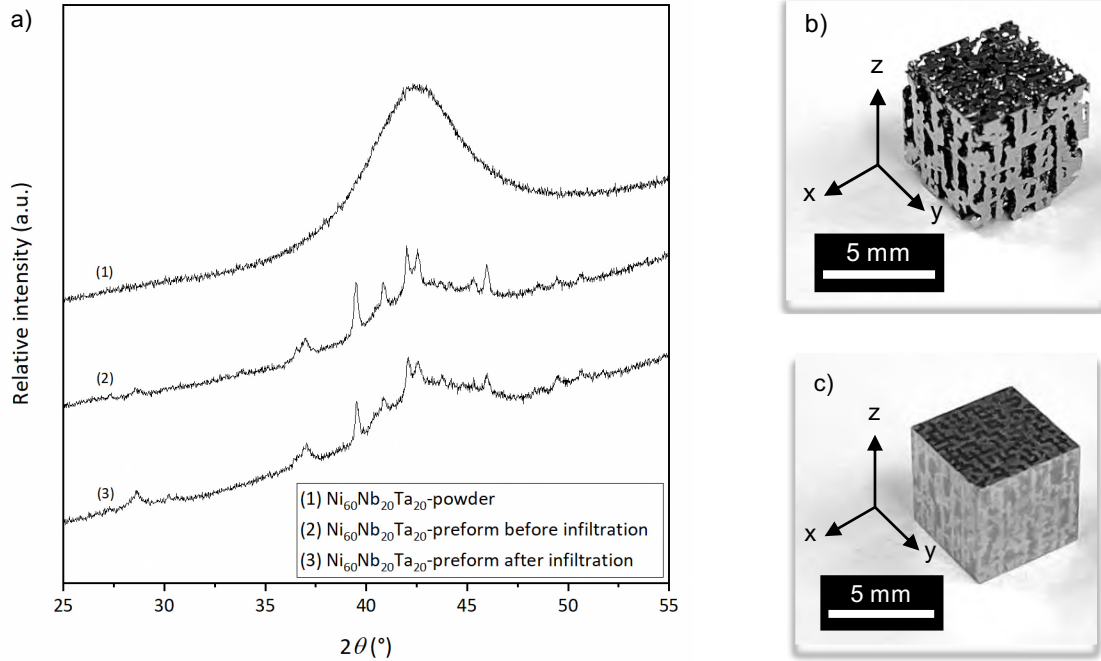


Figure 1: Results of (a) the XRD measurements with the pattern of (1) $\text{Ni}_{60}\text{Nb}_{20}\text{Ta}_{20}$ -powder, (2) $\text{Ni}_{60}\text{Nb}_{20}\text{Ta}_{20}$ -preform before infiltration and (3) $\text{Ni}_{60}\text{Nb}_{20}\text{Ta}_{20}$ -preform after infiltration. Samples of (b) $\text{Ni}_{60}\text{Nb}_{20}\text{Ta}_{20}$ -preform before infiltration and (c) MMC infiltrated preform with AlSi12-matrix ($\text{Ni}_{60}\text{Nb}_{20}\text{Ta}_{20}$ -AlSi12).

It shows a broad maximum at 42.5° , which is typical for Ni-Nb-Ta-based metallic glasses [13,27]. The XRD patterns of the $\text{Ni}_{60}\text{Nb}_{20}\text{Ta}_{20}$ -preform before and after the infiltration exhibit crystallization peaks with a low intensity superimposed on the broad maximum. This nano-crystallization occurs during the manufacturing process of the preform by LPBF. Further investigations, carried out in [20], showed that the crystalline fraction is less than 10%. Compared to the resulting XRD pattern of $\text{Ni}_{60}\text{Nb}_{20}\text{Ta}_{20}$ -preform after infiltration in Figure 1(a), the heat during the infiltration process has no influence on the metallic glass and no further crystallization occurred. Figure 1 also shows a sample of the $\text{Ni}_{60}\text{Nb}_{20}\text{Ta}_{20}$ -preform [Figure 1(b)] and infiltrated $\text{Ni}_{60}\text{Nb}_{20}\text{Ta}_{20}$ -AlSi12 MMC [Figure 1(c)]. The laser-based manufacturing of the preform was carried out in z-direction, as was the subsequent infiltration to manufacture the MMC.

Additionally, the infiltration quality was evaluated based on the density of the MMC. For this purpose, the density of the samples, later used for UPS investigations (volume of approx. $5 \times 5 \times 5 \text{ mm}^3$), was compared with the calculated theoretical density. With a reinforcement fraction of $37.72 \pm 0.62\%$ [20], and density of the metallic glass $\rho_{\text{Ni}_{60}\text{Nb}_{20}\text{Ta}_{20}} = 10.72 \pm 0.05 \text{ g/cm}^3$ [20] and AlSi12-matrix $\rho_{\text{AlSi12}} = 2.64 \text{ g/cm}^3$ [21], the theoretical density of the infiltrated MMC is $\rho_{\text{MMC-theoretical}} = 5.69 \pm 0.05 \text{ g/cm}^3$. Whereas the measured density of the MMC samples [Figure 1(c)] is $\rho_{\text{MMC}} = 5.71 \pm 0.04 \text{ g/cm}^3$ and therefore slightly higher than the theoretical density. The difference could be due to the small sample size with locally higher reinforcement fraction of the metallic glass. In

addition, the theoretically calculated density of the MMC is also based on experimentally determined values, which can also lead to deviation. It can be concluded that no significant gas inclusions occurred during the infiltration process and that the preform has been infiltrated completely.

3.2 Microstructure and interfaces

For visual inspection of the infiltration quality, micrographs were taken in infiltration direction [Figure 2(a)] and transversely to infiltration direction [Figure 2(b)] of the MMC.

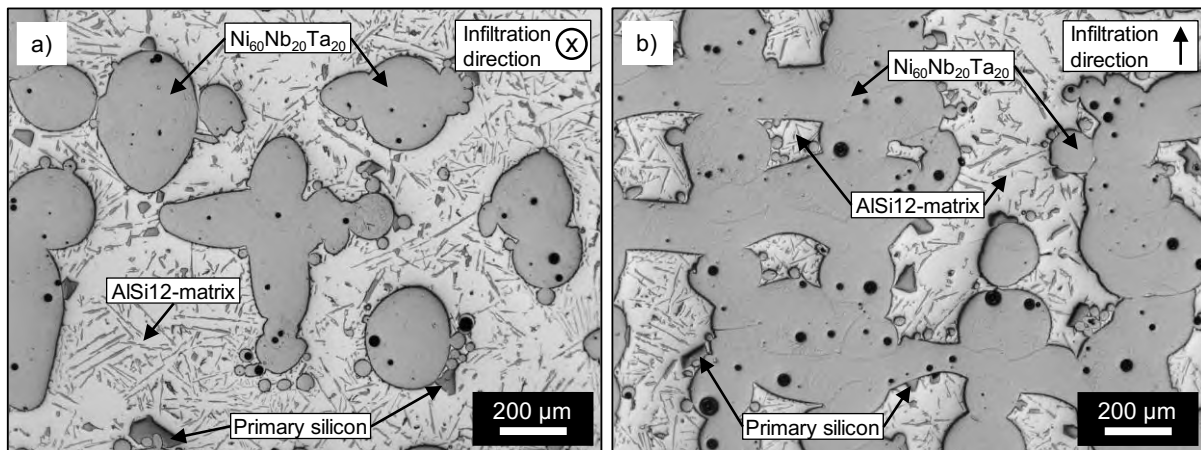


Figure 2: Microscope images of the infiltrated Ni₆₀Nb₂₀Ta₂₀-AlSi12 MMC (a) in infiltration z-direction and (b) transversely to infiltration x-direction.

Both phases of the MMC, the metallic glass Ni₆₀Nb₂₀Ta₂₀ as reinforcement phase and the eutectic AlSi12-matrix, are clearly visible in the microscope images. The phase of the Ni₆₀Nb₂₀Ta₂₀ metallic glass exhibits a different structure in and transversely to infiltration direction. In addition, enclosed gas pores can be seen distributed through the metallic glass phase. Both is caused by the laser-based manufacturing process of the preform [20]. The AlSi12-matrix exhibits a typical homogenous structure with a fine distribution of eutectic Si-lamellae in the α -aluminum phase [28]. Some primary silicon precipitates have been developed in the AlSi12-matrix, mainly located at the interfaces to the metallic glass. This indicates that the metallic glass acts as a nucleating agent for the silicon contained in the matrix alloy. Nucleation of the primary silicon phase at the reinforcement phase is often observed in composites with AlSi-based matrix alloys [1]. The interface between the metallic glass and the AlSi12-matrix does not exhibit a distinct reaction layer on a macroscopic level, which could lead to a deterioration of the composite properties due to a degradation of the reinforcing phase or embrittlement [1,29]. Also, in [30–32] an interface without reaction layers between the metallic glass and the matrix material is observed in sintered composites with metallic glass particles. In [33,34], metallographic micrographs of composites with reinforcements of metallic glass produced by melting metallurgy also show no reaction layers between the metallic glass and the AlSi12-matrix.

Furthermore, the microscope images confirm a good infiltration quality of the preform with the AlSi12-matrix, as no pores or cavities are visible in the AlSi12 phase. Even the smallest areas in between the $\text{Ni}_{60}\text{Nb}_{20}\text{Ta}_{20}$ -preform are filled with matrix material, which can be attributed to the high castability of the AlSi12-matrix [21]. Thus, the composite could be manufactured with comparatively low infiltration pressures [35,36].

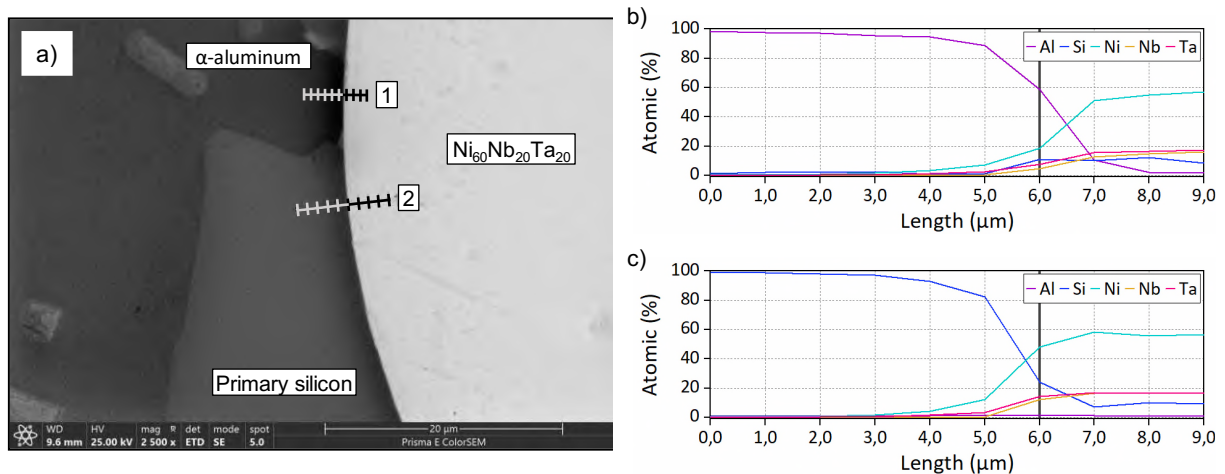


Figure 3: (a) SEM image of the $\text{Ni}_{60}\text{Nb}_{20}\text{Ta}_{20}$ -AlSi12 MMC with the EDX scanning line across the interfaces. Line 1 crosses the interface of α -aluminum – $\text{Ni}_{60}\text{Nb}_{20}\text{Ta}_{20}$ and line 2 the interface of primary silicon – $\text{Ni}_{60}\text{Nb}_{20}\text{Ta}_{20}$. Results of line spectrum with the atomic content of the elements over the length is shown for (b) line 1 and (c) line 2. The position of the interface is marked with a black line at 6 μm .

Figure 3(a) shows the SEM image of the $\text{Ni}_{60}\text{Nb}_{20}\text{Ta}_{20}$ -AlSi12 MMC, in which the phases of the metallic glass $\text{Ni}_{60}\text{Nb}_{20}\text{Ta}_{20}$ and AlSi12-matrix, consisting of primary silicon and α -aluminum, can be seen. Also included are the EDX scanning lines labeled with 1 and 2, where measurements were carried out at ten points equally distributed over a length of 9 μm . Line 1 starts in the α -aluminum phase and crosses the interface to the metallic glass $\text{Ni}_{60}\text{Nb}_{20}\text{Ta}_{20}$, whereas line 2 starts in the primary silicon and ends in the metallic glass. The atomic content of each element over the length is plotted for line 1 in Figure 3(b) and line 2 in Figure 3(c). The EDX scanning lines confirm the visual evaluation. Whereas line 1 has an atomic content of 98.4% Al and 1.3% Si at its starting point, which can be assigned to α -aluminum, line 2 has an atomic content of 99.0% Si and 0.8% Al at its starting point, which corresponds to primary silicon. The aluminum in line 1 and silicon in line 2 decreases slightly with increasing length as they approach the interface of the metallic glass. In both cases, at 4 μm , the elements of metallic glass nickel, niobium and tantalum begin to increase. It can be observed that the atomic content of silicon also starts to increase in line 2. In the interface area between 5 μm and 6 μm , a superposition of all existing elements occurs except for the aluminum in line 2, which does not exceed a maximum value of 1.6% over the entire scan. After the interfacial area, in line 1 the elements reach final atomic contents of 56.9% Ni, 16.1% Nb, 17.1% Ta and a residual atomic content of 1.6% Al. It is noticeable

that in the metallic glass phase the silicon content increased to 8-12%. In line 2 the elements reach final values of 56.7% Ni, 16.4% Nb, 16.8% Ta and a residual atomic content of 0.7% Al. It also remains a silicon content of 7-10% in the metallic glass. Since a diffusion coefficient of only $0.23 \times 10^{-22} \text{ m}^2/\text{s}$ [37] was measured for silicon in metallic glass with alloy composition $\text{Fe}_{40}\text{Ni}_{40}\text{B}_{20}$ at a temperature of 600K, diffusion is probably not the reason for the silicon found within the metallic glass. It is more likely that a peak overlap of the Si-K line and Ta-M line occurred at 1.7 keV during the EDX scan and the peaks are not identified and quantified correctly by the software [38].

In the interfacial areas, the individual elements of the matrix are superimposed with those of the metallic glass in a range of about $3 \mu\text{m}$. This mixing could indicate the development of an interdiffusion layer between the two phases, also observed in [39] at the interface between a $\text{Ni}_{60}\text{Nb}_{20}\text{Ta}_{20}$ metallic glass and an AlSi12-matrix. Such thin interdiffusion layers induce good interfacial bonding between the two phases, resulting in efficient load transfer from the matrix to the reinforcing phase [1,40].

3.3 Mechanical properties

UPS measurements were carried out to determine the Young's modulus and the Poisson's ratio of the $\text{Ni}_{60}\text{Nb}_{20}\text{Ta}_{20}$ -AlSi12 MMC. This method is intended to provide a reliable value for elastic properties, since the determination of Young's modulus from compression tests is influenced by the sensitivity of the experimental setup and setting effects caused by friction between sample and testing tool. Measurements were carried out in infiltration direction (z-direction) and transversely to infiltration direction (x- and y-direction). The results of the Young's modulus (E) and the Poisson's ratio (ν) as well as the sonic speed of longitudinal waves (v_L) and transversal waves (v_T) are presented in Table 3. The listed values are the calculated arithmetic average of all five measured samples and their standard deviation.

Table 3: Results of Young's modulus (E), Poisson's ratio (ν) and sonic waves (v_L , v_T) measured via ultrasound phase spectroscopy (UPS) on $\text{Ni}_{60}\text{Nb}_{20}\text{Ta}_{20}$ -AlSi12 MMC in infiltration direction (z-direction) and transversely (x- and y-direction).

	E (GPa)	ν (-)	v_L (m/s)	v_T (m/s)
x – direction [100]	95.80 ± 3.10	0.335 ± 0.012	5035.62 ± 35.91	2506.98 ± 67.95
y – direction [010]	96.15 ± 2.94	0.328 ± 0.034	5022.51 ± 204.46	2518.70 ± 81.49
z – direction [001]	99.26 ± 1.83	0.323 ± 0.010	5015.47 ± 45.62	2563.49 ± 47.18

The results show that the Young's modulus along z-direction, and thus along the preform building and infiltration direction, is slightly higher than in x- and y-direction. This can be attributed to the

inhomogeneous structure of the $\text{Ni}_{60}\text{Nb}_{20}\text{Ta}_{20}$ -preform caused by the manufacturing process. No significant difference of Poisson's ratio can be seen in the three measured directions considering the standard deviation. Thus, neither the structure of the $\text{Ni}_{60}\text{Nb}_{20}\text{Ta}_{20}$ -preform nor the infiltration direction seems to affect the Poisson's ratio. In [13], the same material system ($\text{Ni}_{60}\text{Nb}_{20}\text{Ta}_{20}$ -AlSi12) was investigated, but the metallic glass had a platelets structure and a reinforcement fraction of only 9.4-14.3%. Within this study, a Young's modulus of 87-93 GPa and Poisson's ratio of 0.31-0.33 was determined in infiltration direction as well as transversely to the orientation of the metallic glass platelets. In addition, a Young's modulus of 85-95 GPa with a Poisson's ratio of 0.31-0.32 was determined transversely to infiltration direction as well as in orientation of the metallic glass platelets by UPS. The values are slightly below the values measured in this work, consequently increasing the reinforcement fraction up to 37.72% did not result in a significantly higher Young's modulus as expected. Also, the Poisson's ratio did not significantly change. In [17], an Al-based MMC reinforced with 30wt.-% metallic glass particles with alloy composition $\text{Ni}_{70}\text{Nb}_{20}$ was manufactured and investigated. It exhibits a Young's modulus of 110 GPa in compression testing, which is also a higher Young's modulus than the MMC studied here despite the lower reinforcement fraction. However, the MMC in this work exhibits a significant increase in Young's modulus up to 28% compared to plain AlSi12, whose value measured by UPS is 77-82 GPa [13,25].

Compression tests were carried out to investigate the behavior and maximum strength of the $\text{Ni}_{60}\text{Nb}_{20}\text{Ta}_{20}$ -AlSi12 MMC in comparison to the plain AlSi12.

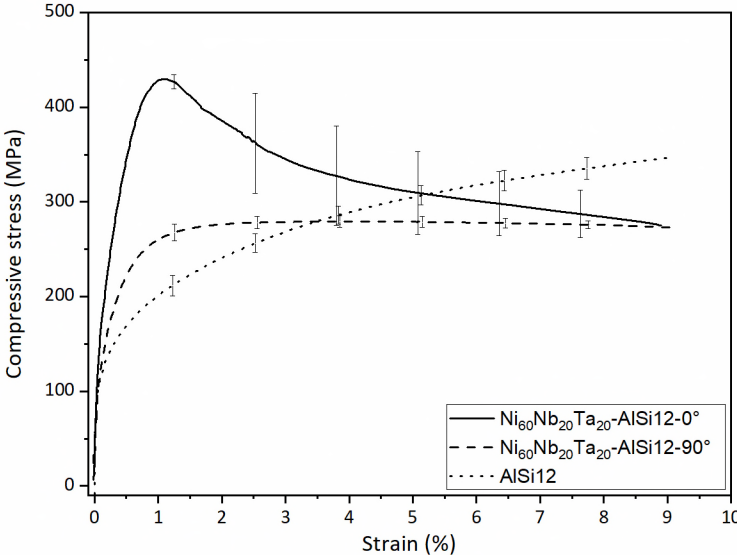


Figure 4: Resulted average compressive stress-strain curves of five samples $\text{Ni}_{60}\text{Nb}_{20}\text{Ta}_{20}$ -AlSi MMC in infiltration direction (0°), five samples transversely to infiltration direction (90°) and five samples plain AlSi12 matrix.

Samples tested in infiltration direction are referred to as $\text{Ni}_{60}\text{Nb}_{20}\text{Ta}_{20}$ -AlSi12- 0° (z-direction) and transversely to infiltration direction $\text{Ni}_{60}\text{Nb}_{20}\text{Ta}_{20}$ -AlSi12- 90° (x- and y-direction). The average resulting

compressive stress-strain curves of the measured samples are shown in Figure 4. The average values of the yield strength $R_{p,0.2}$ (0.2% offset), maximum compressive strength R_m and corresponding compressive strain ϵ are listed in Table 4.

Table 4: Average values of the offset yield strength $R_{p,0.2}$, maximum compressive strength R_m and corresponding compressive strain ϵ of AlSi12, $Ni_{60}Nb_{20}Ta_{20}$ -AlSi-0° and $Ni_{60}Nb_{20}Ta_{20}$ -AlSi12-90°.

	$R_{p,0.2}$ (MPa)	R_m (MPa)	ϵ (at R_m) (%)
AlSi12	157.27 ± 19.85	-	-
$Ni_{60}Nb_{20}Ta_{20}$-AlSi2-0°	294.01 ± 15.80	430.51 ± 4.94	1.12 ± 0.07
$Ni_{60}Nb_{20}Ta_{20}$-AlSi2-90°	186.67 ± 18.82	280.11 ± 7.04	3.36 ± 0.61

The plain AlSi12 reaches an average yield strength of $R_{p,0.2}=157.27$ MPa, which corresponds to the results in literature [13,21]. As expected, the reinforcement by the metallic glass in the AlSi12 causes a significant increase of $R_{p,0.2}$ to 294.01 MPa in $Ni_{60}Nb_{20}Ta_{20}$ -AlSi12-0° and to 186.67 MPa in $Ni_{60}Nb_{20}Ta_{20}$ -AlSi12-90°. The MMC in 0°-direction reaches a maximum compressive strength of $R_m=430.51$ MPa with a corresponding compressive strain of $\epsilon=1.12\%$, the MMC in 90°-direction only reaches a maximum value of $R_m=280.11$ MPa but therefore a significantly higher compressive strain $\epsilon=3.36\%$. In addition, the curves of the two directions show a remarkably different compressive failure behavior. Whereas the stress of the 0°-direction decreases again after reaching the maximum strength, the stress of the 90°-direction remains almost at the same value over the strain. These significant differences between the two directions are caused by the inhomogeneous structure of the $Ni_{60}Nb_{20}Ta_{20}$ -preform due to the manufacturing process. In [20], compression tests were carried out on the $Ni_{60}Nb_{20}Ta_{20}$ -preform and the dependence of the compressive strength on the manufacturing direction was also demonstrated. A dependence of the maximum compressive strength and failure behavior on the orientation of the metallic glass platelets was also observed in [13,39].

The $Ni_{60}Nb_{20}Ta_{20}$ -preform in [20] exhibits a brittle failure behavior, which is typical for metallic glasses and makes them less suitable for the use as monolithic structural components [8]. The failure behavior of the infiltrated $Ni_{60}Nb_{20}Ta_{20}$ -preform in this work confirms that by embedding it in a ductile matrix, the brittle failure behavior of the metallic glass can be compensated by the plasticity of the matrix [1]. Furthermore, a significant increase in maximum compressive strength was achieved in the $Ni_{60}Nb_{20}Ta_{20}$ -AlSi12 MMC compared to the pure $Ni_{60}Nb_{20}Ta_{20}$ -preform, which exhibits a compressive strength of 90 MPa in 0°-direction and of 15 MPa in 90°-direction [20]. However, it should be noted that the MMC is a bulk material, whereas the preform is a lattice structure with only 37% volume fraction.

In [33], metallic glass ribbons Ni-20.6Nb-40.2Ta (wt.-%) were used to reinforce (reinforcement fraction: 20%) an Al-based matrix and an offset yield strength of 163 MPa could be achieved. In [17], a particle reinforced MMC (reinforcement fraction: 30%) with Ni₇₀Nb₃₀ metallic glass and Al-matrix was loaded under compression and reached a maximum compressive strength of 146 MPa. Metallic glass ribbons with alloy composition Ni₆₀Nb₂₀Ta₂₀ were used to reinforce a AlSi12-matrix (reinforcement fraction: 9.4-14.3%) in [13], and an offset yield strength of 149-163 MPa could be achieved. Compared to this, the Ni₆₀Nb₂₀Ta₂₀-AlSi12 MMC in this work achieved a significantly higher compressive strength of 280 MPa and 430 MPa, even though the Young's modulus is comparable low as already discussed. This increase is due to the higher reinforcement fraction of 37% metallic glass and to the interpenetrating structure of the Ni₆₀Nb₂₀Ta₂₀-preform in the MMC. In addition, the high strength of the MMC confirms the good interfacial adhesions between the Ni₆₀Nb₂₀Ta₂₀-preform and AlSi12-matrix, which is generally observed for metal matrix composites with reinforcing elements of metallic glass [17,30,41].

In [18], an interpenetrating MMC of titanium reinforced with a Mg-based metallic glass (reinforcement fraction: 30%) was investigated by performing compression tests. Compared to the porous titanium with a compressive strength of 800 MPa and the monolithic Mg-based metallic glass of 825 MPa, the compressive strength was increased to 1783 MPa in the MMC. Also, a significant enhancement of the plastic deformation capacity up to 31% compressive strain compared to the monolithic metallic glass was achieved. In [19], a porous tungsten was infiltrated with a Zr-based metallic glass (reinforcement fraction: 20%) and investigated by compression tests. The maximum compressive strength of 3450 MPa at 50% compressive strain significantly exceeded that of the tungsten foam (about 1500 MPa at 30%), as well as the monolithic Zr-based metallic glass (about 2000 MPa at 1% strain). Compared to this, the Ni₆₀Nb₂₀Ta₂₀-AlSi12 MMC in this work shows an equally significant increase in compressive strength compared to the plain AlSi12-matrix and Ni₆₀Nb₂₀Ta₂₀-preform. However, the MMC reaches its maximum strength already at 1.1% and 3.4% compressive strain. Since no values of the monolithic Ni₆₀Nb₂₀Ta₂₀ bulk metallic glass are available for investigations under compression, only a comparison with the compressive strain of the Ni₆₀Nb₂₀Ta₂₀-preform in [20] can be made, whereby a comparable increase of compressive strain in the infiltrated MMC can be observed.

In [42], an interpenetrating MMC based on a ceramic foam (reinforcement fraction: 26%) and infiltrated with AlSi10Mg was investigated under compression load. It shows similar failure behavior to the Ni₆₀Nb₂₀Ta₂₀-AlSi12 MMC in 0°-direction in this work and achieves a similar maximum strength of 400 MPa at 1% compressive strain. This indicates that the metallic glass reinforced MMC manufactured in this work can achieve comparable mechanical properties under compression as a MMC reinforced by ceramic.

To the best knowledge of the authors of this publication, this is the first time that an interpenetrating MMC reinforced with a 3D-printed $\text{Ni}_{60}\text{Nb}_{20}\text{Ta}_{20}$ metallic glass preform has been successfully infiltrated with a lightweight AlSi12 alloy. The interpenetrating structure of the metallic glass increased the mechanical strength under compression compared to particle reinforced MMCs, even though the Young's modulus could not be increased by increasing of reinforcement fraction in this case. Also, the plastic deformation capacity and maximum strength were significantly increased compared to the plain $\text{Ni}_{60}\text{Nb}_{20}\text{Ta}_{20}$ -preform and AlSi12-matrix.

4 Conclusion

In this work, a novel interpenetrating MMC with an open porous lattice structure of metallic glass with alloy composition $\text{Ni}_{60}\text{Nb}_{20}\text{Ta}_{20}$ as reinforcement phase and a eutectic AlSi12 as matrix material could be manufactured for the first time successfully by gas pressure infiltration. Process temperature was chosen to be 660 °C and a pressure of 40 bar was applied. The result of the XRD measurement after infiltration shows that no crystallization occurred during the infiltration process. Investigations by digital microscopy and SEM-EDX on micrographs show a high infiltration quality and good interfacial bonding between the metallic glass and matrix without forming a reaction layer. Good interfacial adhesion is confirmed by the results of the compression tests. The $\text{Ni}_{60}\text{Nb}_{20}\text{Ta}_{20}$ -AlSi12 MMC has a strength of 430.51 MPa in z-direction and 280.11 MPa in x- and y-directions. As expected, a significantly higher strength is obtained in the MMC reinforced with metallic glass than in the pure AlSi12-matrix. Also regarding to particle reinforced MMCs, a comparatively higher strength could be achieved with the interpenetrating structure in this work. The behavior under pressure differs between z- and x-/y-direction, which can be attributed to the inhomogeneous structure of the $\text{Ni}_{60}\text{Nb}_{20}\text{Ta}_{20}$ -preform caused by the laser-based manufacturing process. The Young's modulus and Poisson's ratio is with 95.80 GPa and 0.335 in x-direction, 96.15 GPa and 0.328 in y-direction and 99.26 GPa and 0.323 in z-direction comparable low and could not be increased by a higher volume fraction of the metallic glass.

5 Acknowledgments

The authors are thankful to Fraunhofer Institute IFAM (Dresden, Germany) and Nanoval GmbH & Co.KG (Berlin, Germany) for producing the metallic glass alloy and powder. Further, the authors are especially thankful to Steffen Czink from the research group "Production and Component Behavior" (Institute of Applied Materials - Materials Science and Engineering) at Karlsruhe Institute of Technology for carrying out the LPBF procedure. Also, special thanks to the Chair of Solid State Chemistry (Institute of Physics) at Augsburg University for providing their XRD equipment and to S. Schmitt for his technical

and experimental support. The financial support of the German Research Foundation (DFG) within the project WE 4273/19-1 is gratefully acknowledged.

6 References

- [1] Chawla N, Chawla KK. *Metal Matrix Composites*. Boston, MA: Springer US; 2006.
- [2] Clarke DR. Interpenetrating Phase Composites. *Journal of the American Ceramic Society* 1992;75(4):739–58. <https://doi.org/10.1111/j.1151-2916.1992.tb04138.x>.
- [3] Jayalakshmi S, Gupta M. *Metallic amorphous alloy reinforcements in light metal matrices*. Cham: Springer; 2015.
- [4] Polmear IJ, StJohn D, Nie J-F, Qian M. *Light alloys: Metallurgy of the light metals*. 5th ed. Kidlington, Oxford, Cambridge, MA: Butterworth-Heinemann; 2017.
- [5] Suryanarayana C. Metallic glasses. *Bulletin of Materials Science* 1984;6(3):579–94. <https://doi.org/10.1007/BF02744086>.
- [6] Inoue A, Shen B, Koshiba H, Kato H, Yavari AR. Cobalt-based bulk glassy alloy with ultrahigh strength and soft magnetic properties. *Nature Materials* 2003;2(10):661–3. <https://doi.org/10.1038/nmat982>.
- [7] Schroers J. Processing of bulk metallic glass. *Advanced Materials* 2010;22(14):1566–97. <https://doi.org/10.1002/adma.200902776>.
- [8] Ashby M, Greer A. Metallic glasses as structural materials. *Scripta Materialia* 2006;54(3):321–6. <https://doi.org/10.1016/j.scriptamat.2005.09.051>.
- [9] Scudino S, Surreddi KB, Sager S, Sakaliyska M, Kim JS, Löser W et al. Production and mechanical properties of metallic glass-reinforced Al-based metal matrix composites. *Journal of Materials Science Letters* 2008;43(13):4518–26. <https://doi.org/10.1007/s10853-008-2647-5>.
- [10] Dudina DV, Georgarakis K, Li Y, Aljerf M, LeMoulec A, Yavari AR et al. A magnesium alloy matrix composite reinforced with metallic glass. *Composites Science and Technology* 2009;69(15-16):2734–6. <https://doi.org/10.1016/j.compscitech.2009.08.001>.
- [11] Siegrist ME, Löffler JF. Bulk metallic glass–graphite composites. *Scripta Materialia* 2007;56(12):1079–82. <https://doi.org/10.1016/j.scriptamat.2007.02.022>.
- [12] Dudina DV, Georgarakis K, Aljerf M, Li Y, Braccini M, Yavari AR et al. Cu-based metallic glass particle additions to significantly improve overall compressive properties of an Al alloy. *Composites Part A: Applied Science and Manufacturing* 2010;41(10):1551–7. <https://doi.org/10.1016/j.compositesa.2010.07.004>.

- [13] Lichtenberg K, Weidenmann KA. Innovative aluminum based metallic glass particle reinforced MMCs produced by gas pressure infiltration. *Materials Science Forum* 2015;825-826:101–8. <https://doi.org/10.4028/www.scientific.net/MSF.825-826.101>.
- [14] Scudino S, Liu G, Prashanth KG, Bartusch B, Surreddi KB, Murty BS et al. Mechanical properties of Al-based metal matrix composites reinforced with Zr-based glassy particles produced by powder metallurgy. *Acta Materialia* 2009;57(6):2029–39. <https://doi.org/10.1016/j.actamat.2009.01.010>.
- [15] Cytron SJ. A metallic glass-metal matrix composite. *Journal of Materials Science Letters* 1982;1(5):211–3. <https://doi.org/10.1007/BF00724898>.
- [16] Li J-G. Wetting of ceramic materials by liquid silicon, aluminium and metallic melts containing titanium and other reactive elements: A review. *Ceramics International* 1994;20(6):391–412. [https://doi.org/10.1016/0272-8842\(94\)90027-2](https://doi.org/10.1016/0272-8842(94)90027-2).
- [17] Yu P, Kim KB, Das J, Baier F, Xu W, Eckert J. Fabrication and mechanical properties of Ni–Nb metallic glass particle-reinforced Al-based metal matrix composite. *Scripta Materialia* 2006;54(8):1445–50. <https://doi.org/10.1016/j.scriptamat.2006.01.001>.
- [18] Sun Y, Zhang HF, Wang AM, Fu HM, Hu ZQ, Wen CE et al. Mg-based metallic glass/titanium interpenetrating phase composite with high mechanical performance. *Applied Physics Letters* 2009;95(17):171910. <https://doi.org/10.1063/1.3257699>.
- [19] Zhang H, Wang A, Li H, Sun W, Ding B, Hu Z et al. Quasi-static compressive property of metallic glass/porous tungsten bi-continuous phase composite. *Journal of Materials Research* 2006;21(6):1351–4. <https://doi.org/10.1557/jmr.2006.0166>.
- [20] Dittmann K, Czink S, Dietrich S, Trauth A, Weidenmann KA. Laser-Based Additive Manufacturing and Characterization of an Open-Porous Ni-Based Metallic Glass Lattice Structure (Ni₆₀Nb₂₀Ta₂₀). *3D Printing and Additive Manufacturing* 2022. <https://doi.org/10.1089/3dp.2022.0118>.
- [21] Mondolfo LF. *Aluminum alloys: Structure and properties*. London and Boston: Butterworths; 1976.
- [22] Merzkirch M, Blümel C, Rössler R, Schell KG, Bucharsky EC, Weidenmann KA. Manufacturing and Characterization of Interpenetrating SiC Lightweight Composites. *Procedia CIRP* 2014;18:102–7. <https://doi.org/10.1016/j.procir.2014.06.115>.
- [23] Horny D, Schukraft J, Weidenmann KA, Schulz K. Numerical and Experimental Characterization of Elastic Properties of a Novel, Highly Homogeneous Interpenetrating Metal Ceramic Composite. *Advanced Engineering Materials* 2020;22(7):1901556. <https://doi.org/10.1002/adem.201901556>.

- [24] Wanner A. Elastic modulus measurements of extremely porous ceramic materials by ultrasonic phase spectroscopy. *Materials Science and Engineering: A* 1998;248(1-2):35–43.
[https://doi.org/10.1016/S0921-5093\(98\)00524-3](https://doi.org/10.1016/S0921-5093(98)00524-3).
- [25] Roy S, Stoll O, Weidenmann KA, Nagel A, Wanner A. Analysis of the elastic properties of an interpenetrating AlSi12–Al₂O₃ composite using ultrasound phase spectroscopy. *Composites Science and Technology* 2011;71(7):962–8. <https://doi.org/10.1016/j.compscitech.2011.02.014>.
- [26] German Institute for Standardization. DIN 50106: Testing of metallic materials - Compression test at room temperature. Berlin: Beuth Verlag GmbH; 2016.
<https://doi.org/10.31030/2543152>.
- [27] Lee M, Bae D, Kim W, Kim D. Ni-based refractory bulk amorphous alloys with high thermal stability. *Materials Transactions* 2003;44(10):2084–7.
<https://doi.org/10.2320/matertrans.44.2084>.
- [28] Benkißer G. Gefüge der technischen Nichteisenmetalle und ihre Legierungen: Aluminium und Aluminiumlegierungen. In: Schumann H, Oettel H, editors. *Metallografie*, 14th ed. Weinheim: Wiley-VCH; 2009, 773-916.
- [29] Eustathopoulos N, Mortensen A. Capillary Phenomena, Interfacial Bonding, and Reactivity. In: Suresh S, Mortensen A, Needleman A, editors. *Fundamentals of metal-matrix composites*. Boston: Butterworth-Heinemann; 1993, 42-53.
- [30] Jayalakshmi S, Gupta S, Sankaranarayanan S, Sahu S, Gupta M. Structural and mechanical properties of Ni₆₀Nb₄₀ amorphous alloy particle reinforced Al-based composites produced by microwave-assisted rapid sintering. *Materials Science and Engineering: A* 2013;581:119–27.
<https://doi.org/10.1016/j.msea.2013.05.072>.
- [31] Wang Z, Georgarakis K, Nakayama KS, Li Y, Tsarkov AA, Xie G et al. Microstructure and mechanical behavior of metallic glass fiber-reinforced Al alloy matrix composites. *Sci Rep* 2016;6:24384. <https://doi.org/10.1038/srep24384>.
- [32] Zheng R, Yang H, Liu T, Ameyama K, Ma C. Microstructure and mechanical properties of aluminum alloy matrix composites reinforced with Fe-based metallic glass particles. *Materials & Design* 2014;53:512–8. <https://doi.org/10.1016/j.matdes.2013.07.048>.
- [33] Lee M, Kim JH, Park JS, Kim JC, Kim WT, Kim DH. Fabrication of Ni–Nb–Ta metallic glass reinforced Al-based alloy matrix composites by infiltration casting process. *Scripta Materialia* 2004;50(11):1367–71. <https://doi.org/10.1016/j.scriptamat.2004.02.038>.
- [34] Lee MH, Kim JH, Park JS, Kim WT, Kim DH. Development of Ni-Nb-Ta Metallic Glass Particle Reinforced Al Based Matrix Composites. In: *PRICM-5*. Stafa: Trans Tech Publications Ltd; 2005, p. 3427–3430.

- [35] Davim JP (ed.). Metal matrix composites: Materials, manufacturing and engineering. Berlin/Boston: De Gruyter; 2014.
- [36] Michaud VJ. Liquid-state processing. In: Suresh S, Mortensen A, Needleman A, editors. Fundamentals of metal-matrix composites. Boston: Butterworth-Heinemann; 1993.
- [37] Sharma SK, Macht M-P, Naundorf V. Impurity diffusion in the metallic glass Fe₄₀Ni₄₀B₂₀ measured by SIMS. In: Mazzoldi P, editor. Modifications induced by irradiation in Glasses: Proceedings of Symposium F on Chemical and Physical Modifications Induced by Irradiation in Glasses of the 1991 E-MRS fall conference, Strasbourg, France, November 5 - 7, 1991. Amsterdam: North-Holland; 1992, p. 85–90.
- [38] Suzuki M, Rohde D. Resolving Overlapping Peak Problems with NORAN System 7 Spectral Imaging Software, Application Note: 51188, Thermo Fisher Scientific, Madison, WI, USA (2008); Available from: <https://assets.thermofisher.com/TFS-Assets/CAD/Application-Notes/D10051~.pdf>.
- [39] Lichtenberg K. Metallmatrixverbunde mit Verstärkungselementen aus metallischem Glas Ni₆₀Nb₂₀Ta₂₀: Herstellung und Charakterisierung [PhD Thesis]. Karlsruhe, Germany: Karlsruhe Institute of Technology; 2017.
- [40] Needleman A, Nutt SR, Suresh S, Tvergaard V. Matrix, Reinforcement, and Interfacial Failure. In: Suresh S, Mortensen A, Needleman A, editors. Fundamentals of metal-matrix composites. Boston: Butterworth-Heinemann; 1993, p. 233–250.
- [41] Blank-Bewersdorff M, Köster U, Steinbrink G. Interfaces with improved adhesion in metal matrix/metallic glass composites. *Journal of Materials Science Letters* 1989;8(7):796–8. <https://doi.org/10.1007/BF01730141>.
- [42] Schukraft J, Lohr C, Weidenmann KA. 2D and 3D in-situ mechanical testing of an interpenetrating metal ceramic composite consisting of a slurry-based ceramic foam and AlSi10Mg. *Composite Structures* 2021;263:113742. <https://doi.org/10.1016/j.compstruct.2021.113742>.